# **Nanoscale**



**PAPER** 

View Article Online
View Journal | View Issue



Cite this: Nanoscale, 2022, 14, 4762

# Scalable nanomanufacturing of holey graphene *via* chemical etching: an investigation into process mechanisms

Kun Bi, to †a Dini Wang, to †a Rui Dai, to †a Lei Liu, A Yan Wang, to Yongfeng Lu, to call the Siliang Liao, Ling Ding, Houlong Zhuang and Qiong Nian to \*a Viliang Liao, to Call the Siliang Liao

Graphene with in-plane nanoholes, named holey graphene, shows great potential in electrochemical applications due to its fast mass transport and improved electrochemical activity. Scalable nanomanufacturing of holey graphene is generally based on chemical etching using hydrogen peroxide to form through-the-thickness nanoholes on the basal plane of graphene. In this study, we probe into the fundamental mechanisms of nanohole formation under peroxide etching *via* an integrated experimental and computational effort. The research results show that the growth of nanoholes during the etching of graphene oxide is achieved by a three-stage reduction-oxidation-reduction procedure. First, it is demonstrated that vacancy defects are formed *via* a partial reduction-based pretreatment. Second, hydrogen peroxide reacts preferentially with the edge-sites of defect areas on graphene oxide sheets, leading to the formation of various oxygen-containing functional groups. Third, the carbon atoms around the defects are removed along with the neighboring carbon atoms *via* reduction. By advancing the understanding of process mechanisms, we further demonstrate an improved nanomanufacturing strategy, in which graphene oxide with a high density of defects is introduced for peroxide etching, leading to enhanced nanohole formation.

Received 24th December 2021, Accepted 13th February 2022 DOI: 10.1039/d1nr08437b

rsc.li/nanoscale

# 1. Introduction

Graphene with in-plane nanoholes, also known as holey graphene, has been extensively studied in recent years to improve the performance of graphene-based electrochemical devices. The improved performance is attributed to the abundant mass transport channels provided by the nanoholes and the chemically active edge-carbon atoms surrounding the nanoholes. These new features brought by the in-plane nanoholes can overcome the most inevitable issues, including re-stacking and lack of electrochemical activity, of pristine graphene. As a result, the active specific surface area of graphene can be drastically increased, even if the electrical conductivity is slightly reduced. For instance, Y. Bai *et al.* reported that the electrical

To fabricate holey graphene, the most prevalent nanomanufacturing method is to etch graphene oxide (GO) with oxidative chemicals, such as hydrogen peroxide (H<sub>2</sub>O<sub>2</sub>),<sup>6</sup> nitric acid,<sup>9</sup> and oxygen.<sup>10</sup> Among those etchants, H<sub>2</sub>O<sub>2</sub> has been widely used due to the following advantages. First, it is a green process without any highly aggressive etchants and toxic byproducts. Second, it is a solution-based process, which allows thorough mixing of GO sheets and H<sub>2</sub>O<sub>2</sub> molecules, avoiding non-uniform chemical reactions and facilitating the control of the reactions. The solution product can be directly stored or readily used for further processing, such as hydrothermal synthesis and freeze-drying to obtain free-standing, hierarchical porous structures of holey graphene.<sup>11</sup> Third, it is suitable for

conductivity decreased from 3287 to 1786 S m<sup>-1</sup> after the formation of nanoholes on graphene sheets. However, the volumetric capacitance and rate capability of the thin-film electrodes were largely increased due to the improved ion diffusion kinetics. Similar results can be found in the research on holey graphene-based supercapacitors<sup>4</sup> or lithium-ion batteries.<sup>5</sup> To date, an increasing number of studies have demonstrated the superior performance of holey graphene in the specific surface area,<sup>6</sup> specific capacitance,<sup>7</sup> and charge transfer rate,<sup>8</sup> which are the most significant factors affecting the performance of various electrochemical applications.

<sup>&</sup>lt;sup>a</sup>School of Engineering for Matter, Transport and Energy, Arizona State University, Tempe, AZ, 85287, USA. E-mail: Qiong.Nian@asu.edu

<sup>&</sup>lt;sup>b</sup>Department of Mechanical Engineering, University of Nevada, Reno, NV 89557, USA <sup>c</sup>Department of Electrical & Computer Engineering, University of Nebraska-Lincoln, Lincoln, NE 68588, USA

<sup>&</sup>lt;sup>d</sup>Department of Industrial & Manufacturing Systems Engineering, Iowa State University, Ames, IA 50011, USA

<sup>&</sup>lt;sup>e</sup>School of Chemistry and Chemical Engineering, Wuhan University of Science and Technology, Wuhan 430081, People's Republic of China

<sup>†</sup>All authors contributed equally.

Nanoscale Paper

electrochemical applications since it does not require highcost equipment or a strict environment, which is often seen in the bottom-up methods for the fabrication of semiconductorlevel holey graphene sheets.<sup>12</sup>

Although nanomanufacturing of holey graphene using H<sub>2</sub>O<sub>2</sub> etching has been established experimentally, the process mechanism in terms of the formation of nanoholes remains elusive. Previous studies generally agreed that the etching reactions can be attributed to the chemical oxidation by the etchant. The chemical oxidation breaks the covalent carboncarbon bonds, leads to the formation of carboxylic compounds, and results in carbon atom removal as well as the nucleation and growth of in-plane holes. Due to the high binding energy of the  $\pi$ - $\pi$  conjugation, a long processing time and extreme etching conditions were often utilized. However, J. G. Radich et al. pointed out that the etching reactions could be significantly promoted by pre-existing vacancy defects and local kinetics.<sup>13</sup> They tested the hypothesis by a partial reduction process to generate vacancies and then applied UV irradiation to promote the etching reactions. Although these studies are encouraging, several essential aspects of the formation mechanism of nanoholes on graphene basal planes remain unclear, e.g., how the partial reduction pretreatment generates vacancies, how the atomic vacancies facilitate the etching reactions, and what are the reaction mechanisms between H2O2 and the graphene basal planes with/without pre-existing vacancies. Prior studies claimed that H<sub>2</sub>O<sub>2</sub> tends to activate into hydroxyl radicals to react with the graphene sheets and eventually result in in-plane hole formation.<sup>14</sup> Other researchers are inclined to believe that the hole formation is mainly caused by the oxidizing properties of H<sub>2</sub>O<sub>2</sub> <sup>15</sup> itself. However, no experimental or simulation results have been reported to support these assumptions.

In this study, the fundamental mechanism of nanohole formation in holey graphene under peroxide etching is investigated via an integrated experimental and computational effort. We first demonstrate the formation mechanisms of vacancy defects on GO sheets under partial reduction-based pretreatments using molecular dynamics (MD) simulations. Then, the reactions and products between H2O2 and various forms of graphene (e.g., with and without vacancy defects) are investigated by density functional theory (DFT) calculations. Afterwards, the mechanism for the continuous growth of atomic vacancies into in-plane nanoholes under H2O2 etching is revealed by MD simulations and verified by experiments. Based on our study, we come up with a schematic diagram in Fig. 1 to illustrate how vacancies are generated and then grow into nanoholes under peroxide etching, which will be discussed in three steps in the following sections.

# 2. Results and discussion

First of all, how vacancy defects are formed by a partial reduction-based pretreatment of GO is investigated. It is well known that thermal annealing is a common method for redu-

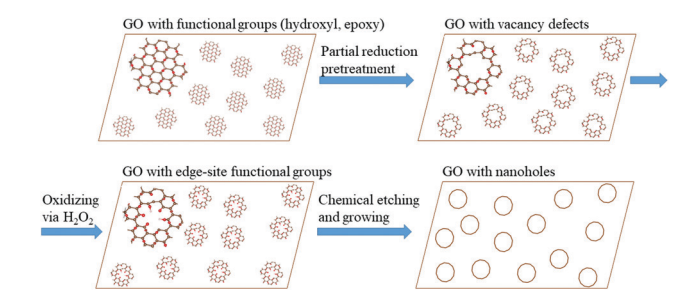


Fig. 1 Schematic diagram of the vacancy defect generation and growth into nanoholes on GO sheets.

cing GO, which removes not only the functional groups but also the in-plane carbon atoms to form vacancy defects.<sup>16</sup> Oxygen-containing functional groups, such as the hydroxyl and epoxy groups, weaken the  $\pi$ - $\pi$  conjugations and increase the activity of neighboring carbon atoms. During annealing, the hydroxyl and epoxy groups remove the carbon atoms from the graphitic lattice to form the gaseous species that eventually leave the system. Therefore, thermal annealing, if used as the partial reduction pretreatment, could generate in-plane vacancy defects on graphene sheets. Herein, MD simulations were carried out to study the carbon-atom removal mechanism during the thermal annealing of GO sheets. In the simulation, a constant temperature increase rate of 8 K fs<sup>-1</sup> was applied on a GO model until it reached a target temperature, and the temperature was kept unchanged to the end. The gaseous products, such as CO, CO2, and H2O, were removed from the simulation box immediately after generation during the whole process.

The initial structure of the GO model (Fig. 2a) shows a graphene sheet randomly anchored by the functional groups that are commonly found in the experiments (i.e., the hydroxyl and epoxy groups). 16,17 After annealing at 1000 K (Fig. 2b), no carbon atom is removed from GO throughout the whole simulation (Fig. 2h), but a few six-atom graphitic rings with rich functional groups are torn off due to the breakage of the sp2 C-C conjugation, resulting in the emergence of the small inplane vacancy defects in these locations. By increasing the target temperature to 1500 K (Fig. 2c), the breakage of the graphitic rings is more evident. The removal of carbon atoms (1%) is observed at this temperature (Fig. 2h). Temperatures of 2000 and 2500 K (Fig. 2d and e) only cause slightly higher atom loss percentages (ca. 2%), but the sizes of in-plane vacancy defects become larger. The formation of these vacancy defects is attributed to not only the reduction reaction of functional groups, but also the physical damage of the graphene lattice by the high kinetic energy input into the model. This can be further verified by the annealing process at 3000 and 3500 K (Fig. 2f and g), which shows severe graphene lattice degradation. The breakage of graphitic rings is not limited to the locations rich of functional groups but extends to the whole lattice. The atom loss percentage surges to ca. 8% at 3000 K and 18% at 3500 K, respectively. Fig. 2h shows that the Paper Nanoscale

Fig. 2 MD simulations of the thermal annealing process of GO at various temperatures: (a) the initial model; (b–g) the models after annealing at 1000, 1500, 2000, 2500, 3000, and 3500 K; (h)  $\rm sp^2$  carbon atom loss percentage of the graphene model with respect to the time step of the simulation.

Oxygen

Carbon

Hydrogen

carbon atom loss percentages at different temperatures all stabilize after a certain time, indicating that no further reduction reaction occurs once the functional groups are consumed. The continuous energy input does not bring about continuous carbon atom removal and the breakage of graphitic rings, indicating that the formation of in-plane vacancies and lattice defects during thermal reduction is determined by the annealing temperature. A high reduction annealing temperature can easily lead to severe lattice degradation. It should be noted that this rule is tenable when the number of pre-occupied oxygen-containing groups is constant. In summary, the MD simulation results suggest that although it can cause the formation of in-plane vacancies, the reduction-based pretreatment cannot sustain a continuous growth of large nanoholes without inducing severe degradation of the neighboring graphitic rings. This is attributed to the completion of carbon atom removal once the reactive functional groups are fully consumed during the thermal reduction process.

The simulation results in Fig. 2 demonstrate the effectiveness and limitation of the partial reduction-based pretreatment process (*i.e.*, thermal annealing) on the formation of vacancy defects. This indicates that a further oxidation reaction is needed to restore reactive functional groups to the atomic sites surrounding vacancy defects if continuous

removal of carbon atoms and thereby the growth of nanoholes are needed.

Herein, it is hypothesized that the  $H_2O_2$ -graphene reaction can add functional groups to the edge sites of vacancy defects. To understand how the  $H_2O_2$  etchant reacts with graphene, and the impact of pretreatment generated vacancy defects on the oxidation reaction kinetics, DFT calculations were conducted. According to prior experimental studies, <sup>15,18</sup> there are two plausible mechanisms of how graphene is oxidized by  $H_2O_2$ : (A)  $H_2O_2$  molecules directly react with graphene and (B)  $H_2O_2$  molecules are first energized to form hydroxyl radicals ('OH), which then react with graphene. In the calculation for mechanism A, an  $H_2O_2$  molecule was placed at the centers of four graphene models, and the results are shown in our previous publication; <sup>19</sup> for mechanism B, a hydroxyl radical was placed on the same locations, and the results are shown in Fig. 3.

The effects of the pre-existing functional groups and pretreatment vacancy defects on the  $H_2O_2$  oxidation reactions were revealed by using four graphene models, *i.e.*, pristine graphene (Fig. 3a), GO (one epoxy group in each unit cell of the graphitic ring, Fig. 3b), graphene with a vacancy defect (a sixatom ring is taken away from the graphene lattice, Fig. 3c), and GO with a vacancy defect (Fig. 3d). Each of the calculations ends until the global energy minimum of the system is Nanoscale Paper

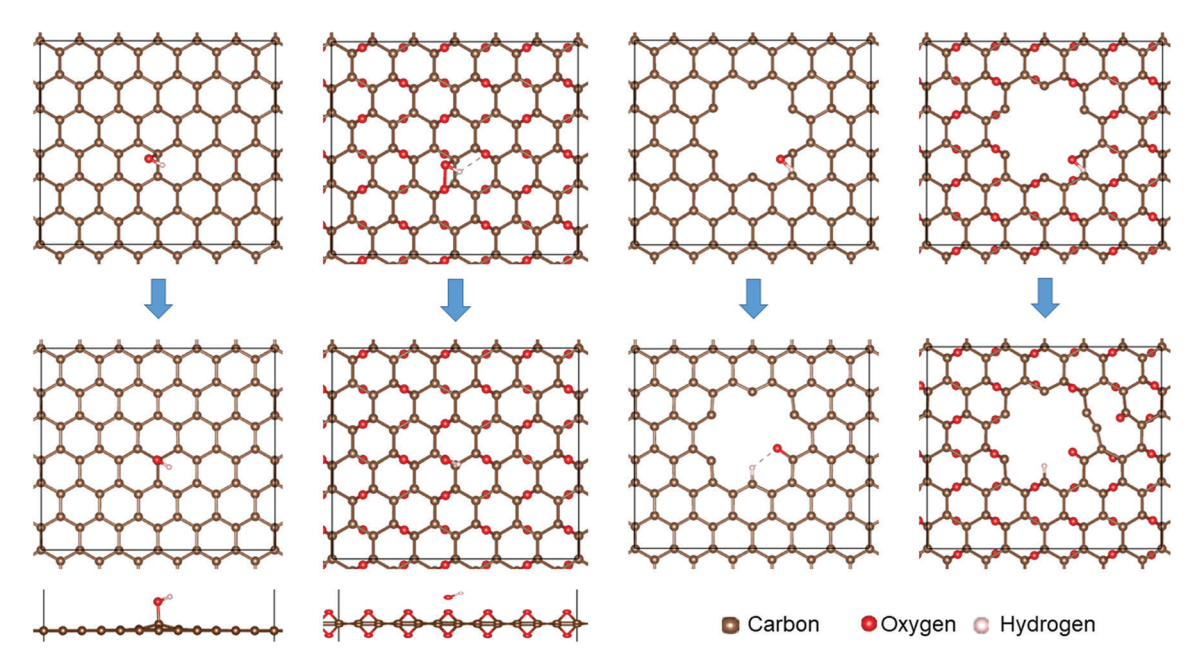


Fig. 3 Models for DFT calculations of the reactions between a hydroxyl radical and (a) graphene, (b) graphene oxide, (c) graphene with a vacancy defect, and (d) graphene oxide with a vacancy defect, respectively.

achieved. The energy change from the initial to the end of the calculation can indicate the possibility of each reaction taking place according to the Boltzmann statistics.

The DFT results in Fig. 3 indicate that the reactions only occur in the cases of graphene and GO with a vacancy defect (Fig. 3c and d), in which the corresponding energy changes are -8.30 and -9.37 eV (Table 1), respectively. Interestingly, in both cases, the edge-site carbon atoms around the vacancy defect are the preferred targets attacked by the hydroxyl radicals. For the graphene model with a vacancy defect (Fig. 3c), the edge-site carbon atoms are anchored by a carbonyl and a hydrogen group. Besides, a hydroxyl group can be anchored onto the graphene basal plane (Fig. 3a), although the energy change is much lower without a pretreatment vacancy defect. For the GO model with a vacancy defect (Fig. 3d), one edge-site carbon atom is anchored by a carbonyl group. This agrees well with prior experimental studies demonstrating that the edge carbon atoms are more chemically active compared to basalplane carbon atoms.20 In addition, as shown in Table 1, the reactions between these edge-carbon atoms and hydroxyl rad-

Table 1 Products and energy changes of the reactions between graphene and hydrogen peroxide or hydroxyl radicals

Initial material	Products with H <sub>2</sub> O <sub>2</sub>	Products with *OH	$\Delta E$ with $H_2O_2$	$\Delta E$ with $^{\bullet}$ OH
Graphene	_	С-ОН	-0.08 eV	-2.06 eV
GO	_	_	-0.12  eV	-0.09  eV
Graphene w/ a vacancy	С≕О, С-Н, С-ОН	C≕O, C-H	−7.06 eV	−8.30 eV
GO w/ a	$C=O, H_2O$	C=O, C-H	−7.03 eV	−9.37 eV
vacancy				

icals are more thermodynamically favorable due to a larger energy change than the reactions with H2O2 molecules (i.e., -7.06 and -7.03 eV energy change<sup>19</sup>). The calculation results suggest that the H2O2 oxidation reaction can be promoted if the H<sub>2</sub>O<sub>2</sub> radicalization process can be catalyzed, which well explains the prior experimental results by J. G. Radich et al. However, without metal or other similar catalysts that are often required to activate H2O2 radicalization, the oxidation reactions are mainly attributed to H<sub>2</sub>O<sub>2</sub> molecules themselves. The products of H<sub>2</sub>O<sub>2</sub> molecules reacting with the edge-carbon atoms are shown in Table 1 as well, including carbonyl, hydroxyl, and hydrogen groups.

For all the reactions aforementioned, the results indicate the adsorption of oxygen-containing groups to the carbon atoms without a direct carbon atom removal, indicating that  $H_2O_2$  can only oxidize the graphene sheets instead of directly taking away carbon atoms. In an actual reaction, a GO sheet may contain the features in local areas similar to those four different graphene models. The areas with vacancy defects are more vulnerable than the intact areas on the GO sheet. The H<sub>2</sub>O<sub>2</sub> molecules prefer to oxidize the carbon atoms surrounding the vacancy defects, forming mainly carbonyl, hydroxyl, and hydrogen groups. When these newly restored functional groups undergo the reduction process again as demonstrated in Fig. 2, the edge-carbon atoms will be removed and vacancy defects (or small size atomic holes) on the GO sheets can grow into larger size nanoholes without inducing severe lattice degradation. In addition, the vacancy-to-nanohole growth process is generally controllable, as it stops once the added functional groups are consumed or the kinetic energy input for the reduction process is suspended. To sum up our computational study shown in Fig. 2 and 3, we consider the partial

Paper Nanoscale

reduction pretreatment process that forms vacancy defects to initiate the hole formation, then H<sub>2</sub>O<sub>2</sub> oxidation restores reactive functional groups and the subsequent repeated reduction process enables the hole growth, as shown in Fig. 1. In practical experiments, these reduction-oxidation-reduction reactions occur continuously so that large nanoholes are formed in multiple locations on a graphene basal plane. This process will be studied next and experimentally verified thereafter.

To confirm whether H<sub>2</sub>O<sub>2</sub> oxidation and the subsequent repeated reduction processes can induce the continuous growth of atomic vacancies into large-size nanoholes, MD simulation of GO under thermal annealing at 1000 K in Fig. 2 is adapted again but coupled with the chemical reactions between H<sub>2</sub>O<sub>2</sub> and GO. In particular, after each time the GO model stabilizes under annealing-based reduction, and additional hydroxyl and carbonyl groups are manually added back to the carbon atoms to mimic the oxidation by H<sub>2</sub>O<sub>2</sub>, which will be followed by another run of the thermal annealing-based reduction process. During the entire simulation, the oxidation and annealing are alternatingly repeated two and three times. Note that, as demonstrated by the DFT calculations, the edge-site carbon atoms surrounding the vacancy defects are chemically active and prone to be oxidized by H<sub>2</sub>O<sub>2</sub>. Therefore, the oxygen-containing functional groups are manually anchored onto those locations, which are assumed to weaken the bonding strength of these carbon atoms.

The MD results are analyzed in Fig. 4. After the first run of thermal annealing at 1000 K for pretreatment (Fig. 4a), several vacancy defects are formed on the graphene basal plane and stabilize within a period of simulation time. Then, the oxidation and the second-round annealing-based reduction are implemented (Fig. 4b). The atomic vacancy on the left side of the graphene model is obviously enlarged into a nanohole. In comparison, no oxidation takes place in the right region of the graphene model (Fig. 4b). No change in the size of this vacancy indicates that oxidation is necessary for the continuous growth of the in-plane holes. This can be further confirmed by repeating the oxidation and annealing processes for another round in Fig. 4c. To quantify the removal of carbon atoms from graphitic rings, the number of sp<sup>2</sup> carbon atoms (orange curve) and overall atoms (carbon atoms plus additional functional groups) (black curve) as a function of simulation time are plotted in Fig. 4d. As observed, both the 1st and 2nd oxidation processes increase the overall atom number in the system in Fig. 4d, which is due to the addition of extra functional groups. However, the number of sp<sup>2</sup> carbon atoms decreases after each oxidation, confirming that the restored functional groups are reactive and can remove the carbon atoms from the graphene basal plane when they are later reduced. This result also indicates that at a relatively low temperature (1000 K), though it cannot create large in-plane nanoholes simply through reduction as demonstrated in

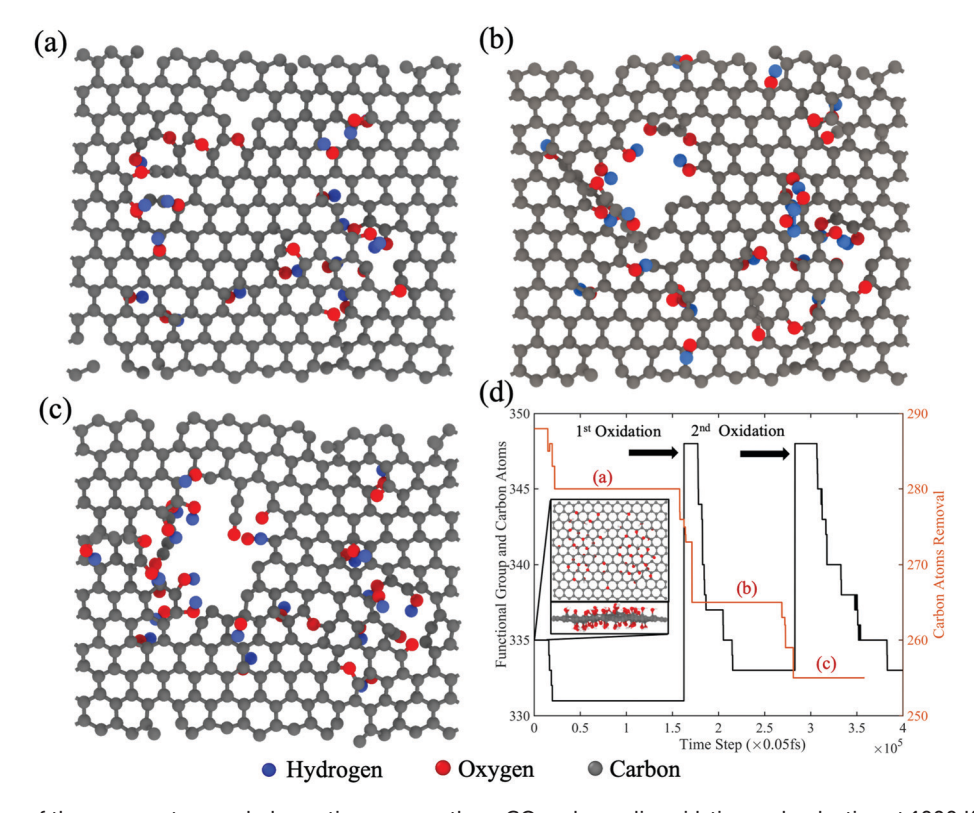


Fig. 4 MD simulations of the vacancy-to-nanohole continuous growth on GO under cyclic oxidation and reduction at 1000 K. (a-c) Images of the models after (a) the reduction-based pretreatment, (b) oxidation plus second-round reduction, and (c) second oxidation plus third-round reduction. (d) The number of carbon atoms in graphitic rings (orange curve) and overall atoms (functional groups and carbon atoms) (black curve) changing with respect to the simulation time. The inset image shows the original GO flake.

Nanoscale Paper

Fig. 2, the H<sub>2</sub>O<sub>2</sub> oxidation can still considerably promote the growth of vacancies-to-nanoholes.

In summary, the encouraging simulation results above suggest that the vacancy defects generated by reduction-based pretreatment play a critical role in manufacturing holey graphene, especially with H<sub>2</sub>O<sub>2</sub> as the etchant. In other words, after the defects are generated during pretreatment, the edgesite carbon atoms tend to become chemically active and react with the etchant more efficiently. These findings will shed light on practical experiments, implying that a defect-forming pretreatment may be able to significantly enhance the etching efficiency, thereby lowering the reaction temperature, shortening the reaction time, minimizing the usage of aggressive chemical etchants, etc.

To verify the simulations above and further study the impacts of the pretreatment-generating vacancy defects, we conducted holey graphene manufacturing experiments using H<sub>2</sub>O<sub>2</sub> as the chemical etchant. Specifically, two batches of holey GO sheets are prepared under different pretreatment conditions. The first batch is obtained by directly heating the mixture of the GO solution and H<sub>2</sub>O<sub>2</sub> without pretreatment. The second batch is first pretreated by microwave heating the GO solution for 360 s at 50 W and then etched with H<sub>2</sub>O<sub>2</sub> under the same conditions as the first batch. The microwave heating pretreatment is selected to achieve the partial reduction of GO according to prior studies.<sup>21</sup> We believe that the density of vacancy defects on GO sheets can vary upon w/ wo pretreatment as demonstrated in our previous publication, 19 so the growth of in-plane nanoholes is different for these two batches of the resulting holey GO sheets.

Microscopic observations of the holey GO sheets collected are shown in Fig. 5. As shown, the holey GO sheet without pretreatment (Fig. 5a) has far fewer in-plane holes than the one with the microwave heating pretreatment (Fig. 5d) in the regions with the same area. To better recognize the nanoholes formed on the GO sheets, the ImageI software was used to recognize the holes and mark them in red color as shown in Fig. 5b and e. In comparison, both the density and size of the holes increase after introducing the pretreatment. Fig. 5c and f further show the density and size of the etched nanoholes. Without the partial reduction-based pretreatment (Fig. 5c), only 3 observed holes are formed in an average size of ~368 nm<sup>2</sup>, and the total holey area is 1105 nm<sup>2</sup> taking around 0.36% of the observed GO sheet (Table 2). The formation of these holes might be attributed to the fact that etching reactions occur on the pre-existing vacancy defects, which were induced in the original exfoliation process. On the other hand, with the pretreatment (Fig. 5f), as many as 137 holes are formed, much more than in the case without pretreatment. The size of the holes varies from  $\sim 50$  to  $\sim 1050$  nm<sup>2</sup>, averagely 161 nm<sup>2</sup> due to a large number of small holes formed. The

Table 2 Hole distribution of holey GO sheets obtained w/wo pretreatment

Treatment	Population	Average size (nm²)	Total area (nm²)	Area percentage
No pretreatment	3	368	1105	0.36%
360 s pretreatment	137	161	22 049	7.24%

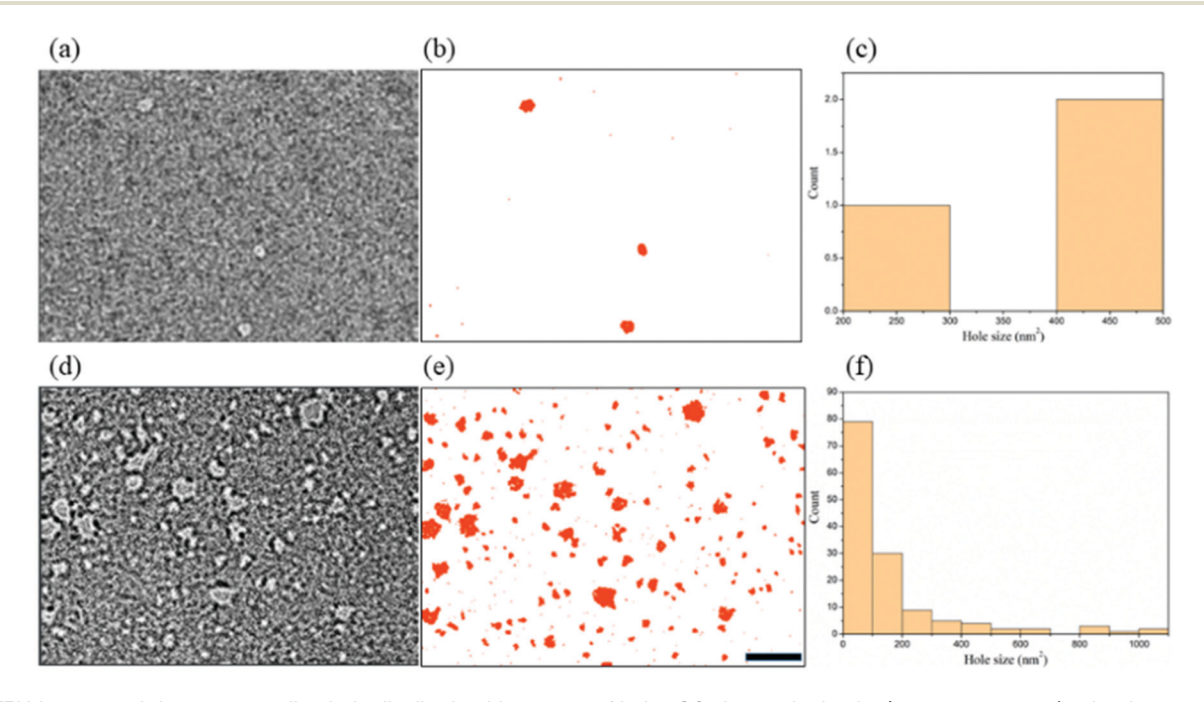


Fig. 5 TEM images and the corresponding hole distribution histograms of holey GO sheets obtained w/wo pretreatment (under the same etching process), showing the effects of preformed vacancy defects on the formation and growth of in-plane nanoholes: (a,b,c) without pretreatment and (d,e,f) pretreated by microwave heating the GO solution for 360 s. Scale bar, 100 nm.

Paper Nanoscale

total holey area is 22 049 nm<sup>2</sup>, occupying around 7.24% of the GO sheet observed. Given the etching reaction time (as detailed in the Experimental section) utilized herein is several minutes, which is much shorter than time periods reported in the prior reports,6 we can conclude that the pretreatment process must have generated a large number of vacancy defects that subsequently grow into large nanoholes. This agrees well with our simulation results above, and previous experimental studies demonstrating that the partial reductions of GO lead to vacancy defects. In addition, the interconnection of the holes could take place during long-time etching as seen in Fig. 5d, implying the hole growth and merging with each other. Our experimental results verify that, with pretreatmentgenerating vacancy defects, holey graphene manufacturing can be significantly promoted even using mild etchants like H<sub>2</sub>O<sub>2</sub>.

Finally, we need to point out that the GO we used in this experiment study is prepared by Hummers' method (see section 3.3) and is very likely to contain a few metal impurities. These impurities might have catalytic effects on the etching process. However, this will not change our conclusion. Because there are metal impurities, the hole formation is not adequate without pretreatment.

#### 3. **Methods**

#### 3.1. DFT calculations

All density functional theory (DFT) calculations were performed using the Vienna Ab initio Simulation Package.<sup>22</sup> The kinetic energy cutoff of the planewaves modeling the electron wavefunctions is set to 500 eV. The Perdew-Burke-Ernzerhof functional<sup>23</sup> is used for treating electron-electron exchangecorrelation interactions. We also adopt the standard version of potential datasets that are created by the projector augmentedwave method<sup>24,25</sup> for approximating the electron-nucleus interactions. A sufficiently large vacuum spacing of 18.0 Å in the cross-plane direction is applied to all the simulation supercells to avoid image interactions. For the k-point sampling, we use a single  $\Gamma$  point, which is sufficient as large supercells are used in our DFT calculations. We optimize the atomic configurations with a force threshold of 0.01 eV  $\mathring{A}^{-1}$ .

#### 3.2. MD simulations

MD simulations are performed using the LAMMPS<sup>26</sup> package with the reactive force-field (ReaxFF) describing the bond association/disassociation process during the thermal annealing of GO sheets. The oxidation of GO sheets is controlled at around 20%. Structural optimization with ReaxFF is performed at room temperature. A Berendsen thermostat with a damping parameter of 100 time-steps is used to control the system temperature. Periodic boundary conditions are applied in the x and y directions with a 10 nm vacuum spacing in the z direction. The time step size is 0.05 fs. Molecular by-products released from the GO sheet are removed periodically every 10 fs to mimic the experimental reduction environment against vacuum. The supercell is first gradually heated from 300 K to

1000 K over a time span of 325 fs, then annealed at 1000 K for around 5 ps, and subsequently quenched to 300 K over a time span of 1 ps. Finally, the supercell is further annealed at 300 K and zero pressure for 3 ps to ensure the complete equilibration of the structure. For the second and third thermal annealing processes, the hydroxyl and epoxy functional groups are only added at the defect edge generated in the previous step while maintaining the same oxidation level. The thermal annealing process is repeated.

#### 3.3. Experimental

A GO aqueous solution was prepared from graphite flakes (50+ mesh, Sigma-Aldrich) by an improved Hummer's method. 27 Then 3 mg mL<sup>-1</sup> GO solution (3 mL) was added into a glass vial with a PTFE cap and processed (pretreatment) in a microwave reactor (Anton Paar Monowave 400, 2.45 GHz) at a constant power of 50 W for 360 s while stirring at a speed of 600 rpm. After cooling, 1 mL of H<sub>2</sub>O<sub>2</sub> (30%) was added into the vial, and then the same microwave process was repeated (etching). To confirm the existence of holes, the GO sheets were characterized using a TEM (FEI Titan, 300/80) at 300 kV.

#### Conclusions 4.

The fundamental mechanisms involved in holey graphene fabrication via chemical etching are investigated. The research results indicate that the formation of nanoholes in graphene basal planes is achieved by a three-stage procedure of reduction-oxidation-reduction, as illustrated in Fig. 1. In particular, the vacancy defects on graphene sheets formed by partial reduction-based pretreatment are preferentially oxidized by H<sub>2</sub>O<sub>2</sub>. After the oxidation, the carbon chains around the defects are anchored by various reactive functional groups, which are then removed along with the neighboring carbon atoms by reduction reactions. This three-stage procedure facilitates the growth of atomic vacancies into large nanoholes on graphene basal planes. It is also demonstrated that a defectforming pretreatment process can significantly promote the etching reactions for holey graphene manufacturing.

### **Author contributions**

This work was devised by QN, DW and RD. KB and DW performed the experimental measurements. KB performed the image processing for the statistical calculations of the fabricated structures. RD conducted computational simulations with assistance from LL, YL and HZ. All authors co-wrote the manuscript.

# Conflicts of interest

There are no conflicts to declare.

Nanoscale Paper

# Acknowledgements

This study was partially supported by NSF grants CMMI-1826392, CMMI-1825576, and CMMI-1825608. We acknowledge the use of facilities within the Eyring Materials Center at Arizona State University supported in part by NNCI-ECCS-1542160.

## References

- 1 Z. Chen, X. An, L. Dai and Y. Xu, *Nano Energy*, 2020, 104762.
- 2 R. Raccichini, A. Varzi, S. Passerini and B. Scrosati, *Nat. Mater.*, 2015, **14**, 271.
- 3 Y. Bai, X. Yang, Y. He, J. Zhang, L. Kang, H. Xu, F. Shi, Z. Lei and Z.-H. Liu, *Electrochim. Acta*, 2016, **187**, 543–551.
- 4 Y. Xu, Z. Lin, X. Zhong, X. Huang, N. O. Weiss, Y. Huang and X. Duan, *Nat. Commun.*, 2014, 5, 4554.
- 5 X. Zhao, C. M. Hayner, M. C. Kung and H. H. Kung, ACS Nano, 2011, 5, 8739–8749.
- 6 Y. Xu, C.-Y. Chen, Z. Zhao, Z. Lin, C. Lee, X. Xu, C. Wang, Y. Huang, M. I. Shakir and X. Duan, *Nano Lett.*, 2015, 15, 4605–4610.
- 7 P. Xu, Q. Gao, L. Ma, Z. Li, H. Zhang, H. Xiao, X. Liang, T. Zhang, X. Tian and C. Liu, *Carbon*, 2019, 149, 452–461.
- 8 J. Zhao, Y.-Z. Zhang, F. Zhang, H. Liang, F. Ming, H. N. Alshareef and Z. Gao, *Adv. Energy Mater.*, 2019, 9, 1803215.
- 9 M. Zhao, Appl. Sci., 2018, 8, 1303.
- 10 L. Liu, S. Ryu, M. R. Tomasik, E. Stolyarova, N. Jung, M. S. Hybertsen, M. L. Steigerwald, L. E. Brus and G. W. Flynn, *Nano Lett.*, 2008, 8, 1965–1970.
- 11 Y. Xu, Z. Lin, X. Zhong, X. Huang, N. O. Weiss, Y. Huang and X. Duan, *Nat. Commun.*, 2014, 5, 1–8.

- 12 X. Dong, N. Hu, L. Wei, Y. Su, H. Wei, L. Yao, X. Li and Y. Zhang, *J. Mater. Chem. A*, 2016, 4, 9739–9743.
- 13 J. G. Radich and P. V. Kamat, ACS Nano, 2013, 7, 5546-5557.
- 14 R. S. Ribeiro, A. M. T. Silva, J. L. Figueiredo, J. L. Faria and H. T. Gomes, *Carbon*, 2013, **62**, 97–108.
- 15 W. Xing, G. Lalwani, I. Rusakova and B. Sitharaman, *Part. Part. Syst. Charact.*, 2014, 31, 745–750.
- 16 D. R. Dreyer, S. Park, C. W. Bielawski and R. S. Ruoff, Chem. Soc. Rev., 2010, 39, 228–240.
- 17 W. Cai, R. D. Piner, F. J. Stadermann, S. Park, M. A. Shaibat, Y. Ishii, D. Yang, A. Velamakanni, S. J. An, M. Stoller, J. An, D. Chen and R. S. Ruoff, *Science*, 2008, 321, 1815–1817.
- 18 M. J. Yoo and H. B. Park, Carbon, 2019, 141, 515-522.
- 19 D. Wang, R. Dai, X. Zhang, L. Liu, H. Zhuang, Y. Lu, Y. Wang, Y. Liao and Q. Nian, *Carbon*, 2020, **161**, 880– 891.
- 20 A. Shen, Y. Zou, Q. Wang, R. A. W. Dryfe, X. Huang, S. Dou, L. Dai and S. Wang, *Angew. Chem.*, 2014, 126, 10980–10984.
- 21 X. Xie, Y. Zhou and K. Huang, Front. Chem., 2019, 7, 355-366.
- 22 G. Kresse and J. Furthmüller, *Comput. Mater. Sci.*, 1996, 6, 15–50.
- 23 J. P. Perdew, K. Burke and M. Ernzerhof, *Phys. Rev. Lett.*, 1996, 77, 3865–3868.
- 24 G. Kresse and D. Joubert, *Phys. Rev. B: Condens. Matter Mater. Phys.*, 1999, 59, 1758–1775.
- 25 P. E. Blöchl, Phys. Rev. B: Condens. Matter Mater. Phys., 1994, 50, 17953–17979.
- 26 B. FrantzDale, S. J. Plimpton and M. S. Shephard, *Eng. Comput.*, 2010, **26**, 205–211.
- 27 D. C. Marcano, D. V. Kosynkin, J. M. Berlin, A. Sinitskii, Z. Sun, A. Slesarev, L. B. Alemany, W. Lu and J. M. Tour, ACS Nano, 2010, 4, 4806–4814.